CFD Letters

Numerical Modelling of Synthetic-Jet-Assisted Mixing

Open Access

Hong Mun Hoh[1], Cheng See Yuan[2,*], Lim Kim Chuan[3]

[1] Faculty of Mechanical Engineering, Universiti Teknikal Malaysia Melaka, Hang Tuah Jaya, 76100 Durian Tunggal, Melaka, Malaysia
[2] Centre for Advanced Research on Energy, Universiti Teknikal Malaysia Melaka, Hang Tuah Jaya, 76100 Durian Tunggal, Melaka, Malaysia
[3] Center for Telecommunication Research & Innovation, Universiti Teknikal Malaysia Melaka, Hang Tuah Jaya, 76100 Durian Tunggal, Melaka, Malaysia

ARTICLE INFO	ABSTRACT
	The aim of the present study is to develop a Computational Fluid Dynamics (CFD) model of synthetic-jet-assisted fluid mixer. A geometric model which consists of a mixing channel with a pair of synthetic jet actuators was created. The diaphragm motion of the synthetic jet actuators was realized by a moving mesh method. Dye solution and water were introduced into the fluid mixer from two different inlets. Mixing degree was numerically predicted as the result of the CFD model. Verifications were performed to examine the sensitivity of the model to temporal and spatial resolutions. The results were validated against experimental data and a good agreement was achieved. The overall results indicated that the time-step size affected the mixing degree significantly. The mesh resolution only has slight influence on the mixing degree.

1. Introduction

A synthetic jet is a zero-net-mass-flux (ZNMF) jet, which can be produced by the synthetic jet actuator (SJA). The actuator consists of a closed volume cavity with an oscillating diaphragm at one side and an orifice on the other. As a result of the oscillating motion of the diaphragm, the processes of expulsion and ingestion of fluid are created around the orifice exit. Subsequently, a train of vortical structures are generated and propagated further downstream from the orifice exit. These vortical structures will interact with the ambient fluid and entrain them into the jet. Due to their distinctive mechanism, the vortical structures induced from SJA could be beneficial to some applications including mixing enhancement [1–4], flow separation control [5,6], thermal management [7,8], jet vectoring [9, 10], aero-optics [11, 12] and cavity oscillations [13].

Past studies have shown that the use of synthetic jet can improve the mixing performance of fuel-air microjets or fluid mixing devices significantly [3,4], [14–18]. Xia and Zhong [2] have carried out an experimental study to investigate the effect of a lateral piston-typed synthetic jet actuator pair on the mixing between two water streams of same flow rate in a planar mixing channel. They found that

---

* Corresponding author.
E-mail address: cheng@utem.edu.my (Cheng See Yuan)

the good mixing between the two water streams is attributed to the vigorous interaction between the opposing vortex pairs generated by the lateral synthetic jet actuator pair with high excitation frequencies or stroke ratio. Xia and Zhong [17] showed that the multiple piston-typed synthetic jet pairs enhance the mixing performance in the mixing channel at a low net flow Reynolds number. They have also found that staggered lateral synthetic jet (LSJ) actuator pair shows a better mixing performance than the opposing LSJ actuator pair at certain range of excitation frequencies and stroke ratio [3]. Xia and Zhong [4] further extended their experimental study [17] to investigate the effect of three lateral synthetic jet pairs on the mixing enhancement in a planar mixing channel at three different net flow Reynolds numbers. In addition, similar studies have been carried out numerically by Mautner [14] and Tesař [15].

Numerical approaches by using CFD has been proved very effective for analysing heat and fluid flow in sufficient detail [19, 20]. However, numerical studies of synthetic jets in mixing enhancement between fluids are relatively fewer as compared to the numerous experimental studies. Although experimental studies have provided a good understanding of flow physics in enhancing fluid mixing, some of the important jet characteristics such as jet blowing velocity or mass flow rate through the orifice are difficult to obtain experimentally. Therefore, the aim of this paper is to develop a Computational Fluid Dynamics (CFD) model for improving the understanding on the jet characteristics in the aspect of mixing enhancement. In the present paper, a geometric model which consists of a mixing channel with a pair of synthetic jet actuators was created. The diaphragm motion of the synthetic jet actuators was realized by a moving mesh method. Dye solution and water were introduced into the fluid mixer from two different inlets. Mixing degree is numerically predicted as the result of the CFD model. The computational results obtained by using different applied time-step sizes and mesh sizes are validated against the experimental results.

2. Methodology

For the stated objectives, a commercial Computational Fluids Dynamic (CFD) software ANSYS, Inc is used to simulate all the cases. The pressure-based solver is utilised to obtain the solution of unsteady incompressible flow 3D model. Viscous laminar model is applied to all the cases. Based on the principle of conservation of mass and momentum, the incompressible governing equations are derived from the continuity equation,

$$\nabla . \vec{u} = 0, \tag{1}$$

and the momentum equations,

$$\rho \frac{\partial \vec{u}}{\partial t} + \rho \vec{u} \cdot \nabla \vec{u} = -\nabla P + v \nabla^2 \vec{u} \tag{2}$$

where, ρ is the fluid density, $\vec{u}$ is the fluid velocity vector, P is the fluid pressure, v is the kinematic viscosity and ∇ is the Laplacian operator. In addition, species transport equations are used to estimate the local mass fraction of each species (dye or water in the present study), Y_i, through the solution of a convection-diffusion equation for the ith species. The general form of the equation is shown as below:

$$\frac{\partial}{\partial t} (\rho Y_i) + \nabla \cdot (\rho \vec{u} Y_i) = -\nabla \cdot \vec{J_i} + R_i + S_i \tag{3}$$

where, R_i is the net rate of production of species i by chemical reaction, S_i is the rate of creation by addition from the dispersed phase and user-defined sources, and $\vec{J_i}$ is the diffusion flux of species i, which shown as

$$\vec{J_i} = -\rho D_{i,m} \nabla Y_i \qquad (4)$$

where, $D_{i,m}$ is the diffusion coefficient for species i in the mixture. In the present study, PISO scheme is chosen as the solution method while second order upwind scheme is chosen for the spatial discretization of pressure, momentum, dye and energy. First order implicit is used for the transient formulation.

2.1 Physical Properties

In the present study, the physiochemical process between dye solution and water is carried at a temperature of 300K. Under a temperature of 300K, the physical properties of water can be assumed for the whole system when the saturation concentration of the Rhodamine B in water is very low [21]. As both of the fluids have the same physical properties (as shown in Table 1), the dye solution with a concentration of 1 (mass fraction) is corresponded to the Rhodamine B solution with a very low concentration (0.2 mg/L) that utilized by the experimental study [2]. The diffusion coefficient of dye is considered to be 3.6 x 10^{-10} m/s [22].

Table 1
Physical properties of water used in the present study

Physical properties	Value
Density	998.2 kg/m^3
Dynamic viscosity	0.001003 kg/ms
Molecular weight	18.0512 $kg/kgmol$

2.2 Computational geometry

A baseline model of a mixing channel with a pair of lateral synthetic jet (LSJ) actuators is created according to the experiment setup [2]. The dimensions of the baseline model are measured in *mm* and shown in Figure 1.

The rectangular mixing channel has a depth of 40 mm (in z-direction). Both of the actuators have the same dimensions and the jet cavity has a depth of 126 mm. The rectangular orifice has the same depth as the mixing channel. The centre of jet cavity has an offset of 4 mm (positive y-direction) from the centre of orifice, which is the origin of coordinated system of the geometrical model. Due to the limitation of the computational resources, a plane of symmetry is created in *xy*-plane and only half of the model will be used for the present study (as shown in Figure 2). The dye solution and water are introduced into the mixing channel via the left and right inlet, respectively.
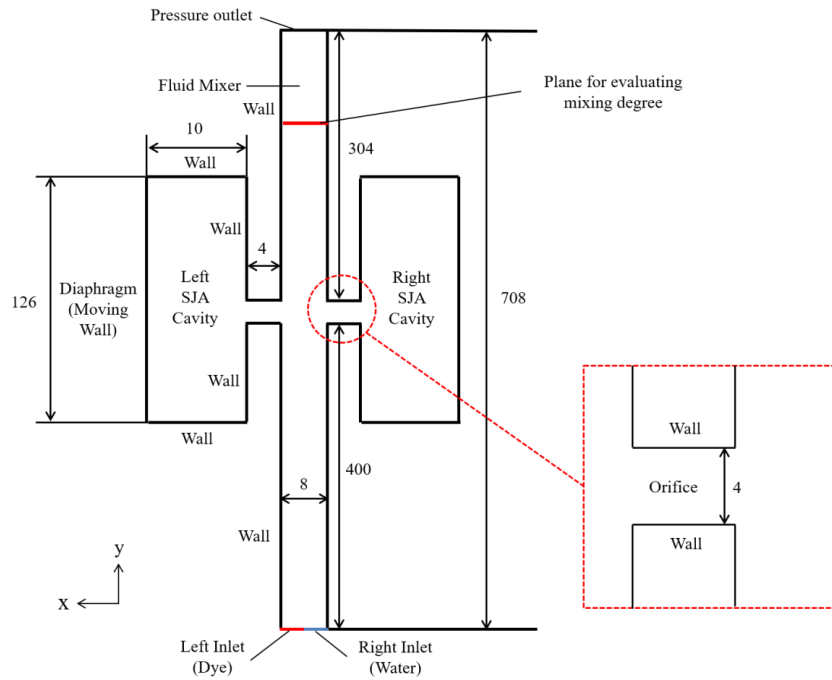
Fig. 1. 2D Schematic diagram of the geometric model
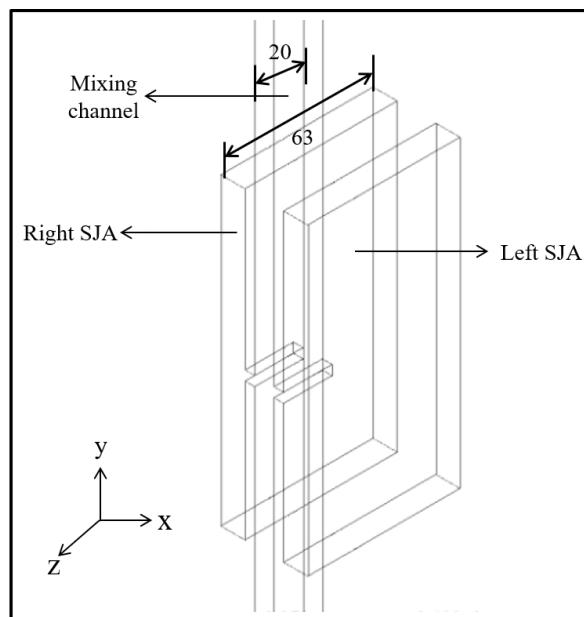
Fig. 2. A 3D schematic diagram of the geometric model

Both of the actuators are operated with the same displacement but in an opposite phase. The bottom of the cavity is assumed to be an oscillating piston and the oscillation movement is defined by Eq. (5).

$$x_{wall} = -a.\cos(2\pi f.t) \tag{5}$$

where, x = nondimensional Cartesian coordinate in x-direction, a = amplitude of the cavity wall oscillation, f = frequency of the oscillation movement and t = time in second (s).

2.3 Computational Grid

Hexahedral meshes are applied to all the geometric models (Figure 3). The mesh cells are refined around the orifice exit region. Besides, finer mesh cells are also employed in the downstream region of mixing channel where after the fluid flows through the orifice exit region. The total number of the mesh cell is 1870000 (as shown in Table 2).
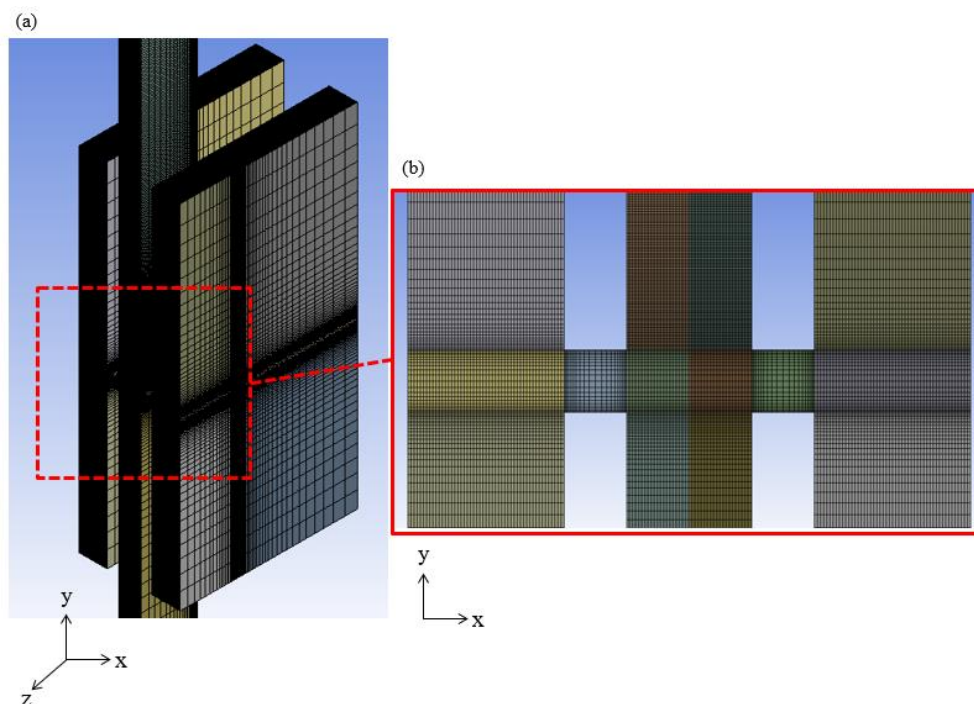
Fig. 3. Meshed model for present study (a) View of three-dimensional (b) View of two-dimensional

Table 2
Number of mesh cells of different region

Region	Mesh cells
	X x Y x Z
Orifice (each)	20 x 20 x 25
Cavity (each)	50 x 100 x 65
Mixing channel	80 x 600 x 25

2.4 Boundary Conditions

The velocity of the fluid is fixed at 0.01 m/s for both left and right inlet. A constant dye concentration with a value of 1 (mass fraction) is applied at the left inlet whereas the right inlet contained only pure water. The direction of the flow is defined normal to the boundary. For the outlet, pressure-outlet boundary condition is chosen with a specified value of 101.325 kPa. For all the walls, a no-slip boundary condition is imposed, and zero diffusive flux of species is specified.

2.5 Dimensionless Parameters

The mixing degree is related with the following functional expression,

Mixing Degree = $f(\overline{U}_n, \overline{U}_j, h, d, f, \rho, \mu)$,

where, $\overline{U}_n$ = time-averaged velocity across the mixing channel, $\overline{U}_j$ = time-averaged jet velocity during the expulsion stroke, h = width of the mixing channel (measured in xy-plane), d = width of the orifice (measured in xy-plane), f = actuation frequency of the oscillating diaphragm in the SJA, ρ = density of the fluid and μ is the dynamic viscosity of the fluid. Under the condition of fixing $\overline{U}_n$, h , and ρ as the repeating parameters, the mixing degree can be governed by four independent dimensionless parameters, which are net flow Reynolds number, Re_n, dimensionless stroke length, *L*, Strouhal number, *Str*, and the dimensionless orifice width, *d/h*. The net flow Reynolds number, Re_n is described as

$$Re_n = \frac{\rho h \overline{U}_n}{\mu} \tag{6}$$

and the dimensionless stroke length, *L* can be defined as

$$L = \frac{L_o}{d} = \frac{\overline{U}_j T}{d} = \frac{\overline{U}_j}{df} \tag{...}$$

where, L_o = as the ejected fluid column length from the orifice exit during the expulsion stroke [23]:

$$L_o = \overline{U}_j T \tag{7}$$

where, T = time period of excitation cycle and $\overline{U}_j$ = time-averaged exit velocity based on the integration of expulsion velocity over one period (Smith & Glezer 1998), which is shown in Eq. (8).

$$\overline{U}_j = \frac{1}{T} \int_0^{\frac{T}{2}} u_o(t)\, dt \tag{8}$$

where, $u_o(t)$ refers to the instantaneous stream-wise space averaged velocity at the orifice exit plane. The Strouhal number, *Str* and the dimensionless orifice width, *d/h* are used to determine the level of interaction between two opposing jets produced by the lateral SJA pairs in the mixing channel,

$$Str = \frac{fh}{\overline{U}_n} \tag{9}$$

and velocity ratio, R_v is used to determine the relative strength of the synthetic jet to the mean flow in the mixing channel, which is defined by Eq. (10).

$$R_v = \frac{\overline{U}_j}{\overline{U}_n} \tag{10}$$

3. Result and Discussions

In this numerical study, the ratio between the flow rates in the left and right streams is fixed at 1 and the mean velocity across the mixing channel is kept constant at 0.01 m/s. The net flow Reynolds number, Re_n remains constant at 83, while the Strouhol number, Str is fixed at 0.4. The dimensionless stroke length, L varies from 0 to 8, and the velocity ratio, R_v varies from 0 to 3.2. The actuation frequency of the SJA is fixed at 1 Hz.

3.1 Method of Evaluation

As shown in Figure 1, a plane (red line) is created across the central plane of the mixing channel (Z = 0) at a downstream distance of 104 mm from the origin of the model for evaluating the mixing degree between two fluids. This downstream distance is chosen in correspond to the one used in the experimental study by Xia and Zhong [2]. The quantitative evaluation of the extent of mixing is based on the equation of weighted standard deviation proposed by Glasgow and Aubry [25], which is defined in the following equation,

$$\text{Mixing degree} = 1 - \frac{\sqrt{\sum_{i=1}^{n} \frac{(x_i - \mu)^2}{n}\left(\frac{v_i}{v_{mean}}\right)}}{\mu} \qquad (11)$$

where, x_i is the mass fraction of dye in i^{th} facet, μ = 0.5, the mass fraction of the dye which implies a fully mixed condition of two fluids, v_i is the velocity magnitude in the ith facet, v_{mean} is the mean velocity in across the line inside the mixing channel and n is the total number of facets. Noted that the mass fraction of dye, μ = 0.5 is corresponded to the concentration of 0.1 mg/L Rhodamine B which indicates the fully mixed condition between two fluids in the experiment study [2]. A condition of fully mixing and no mixing between two fluids yields a mixing degree with value of 1 and 0, respectively.

In addition, the time-averaged mixing degree is calculated based on the last 5 oscillation cycles of the SJAs.

3.2 Grid Independence Study

According to Table 3, three different mesh partitions are investigated in the present study. It is found that the time-averaged mixing degree of the three different meshes are nearly similar (as shown in Figure 4 and Table 4).

Table 3
Mesh refinement cases

Mesh designation	Coarse	Medium	Fine
	X x Y x Z	X x Y x Z	X x Y x Z
Orifice (each)	12 x 10 x 25	20 x 20 x 25	30 x 30 x 25
Cavity (each)	50 x 90 x 65	50 x 100 x 65	50 x 110 x 65
Mixing channel	70 x 395 x 25	80 x 600 x 25	120 x 710 x 25
Total mesh	1,282,250	1,870,000	2,890,000
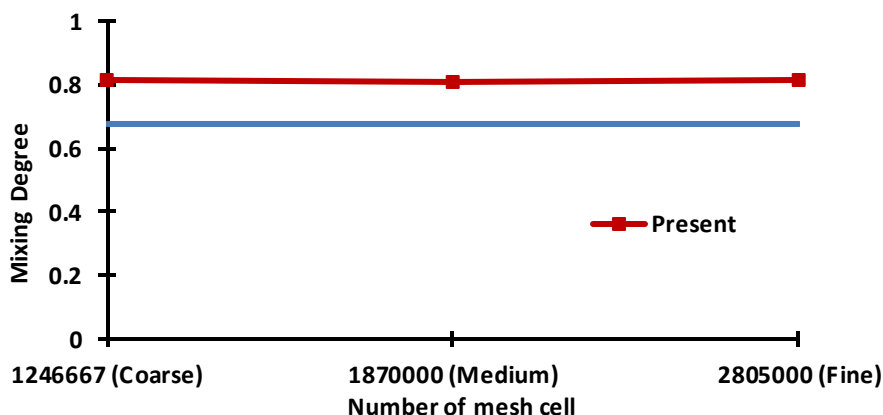
Fig. 4. Comparison of time-averaged mixing degree obtained from different mesh refinement cases and experiment at stroke ratio, L = 4 and velocity ratio, R_v = 1.6

Table 4
Time-averaged mixing degree obtained from cases with three different meshes

Number of mesh cell	Mixing degree [2]	Time-averaged mixing degree (Present study)	Percentage Difference (%)
1,282,250	0.677	0.814	20.20
1,870,000	0.677	0.81	19.54
2,890,000	0.677	0.818	20.77

3.2.1 Near-field region

The concentration contours in Figure 5 show that the flow patterns of both fluids slightly become apparent as the mesh density increases. For both experiment and present study, the phase-averaged velocity fields and vorticity contours depict that the vortices ejected from the left SJA have similar size and propagation distance along the mixing channel in all the cases with different mesh density.

3.2.2 Downstream flow region

The downstream flow patterns near the evaluation plane is shown in Figure 6. The concentration contour near the region of evaluation plane do not affected by the applied mesh density. In the experiment, the partial mixed strips (yellow and blue) are noticeable in the mixing channel, however, these strips are not observed in all three different meshes. Therefore, the time-averaged mixing degree of all the cases are over predicted as the well-mixed region (green) in the channel is larger than the one in experiment.

As a compromise of computational time and spatial resolution around the orifice exit region, medium mesh partition is chosen for further investigation in the present study.
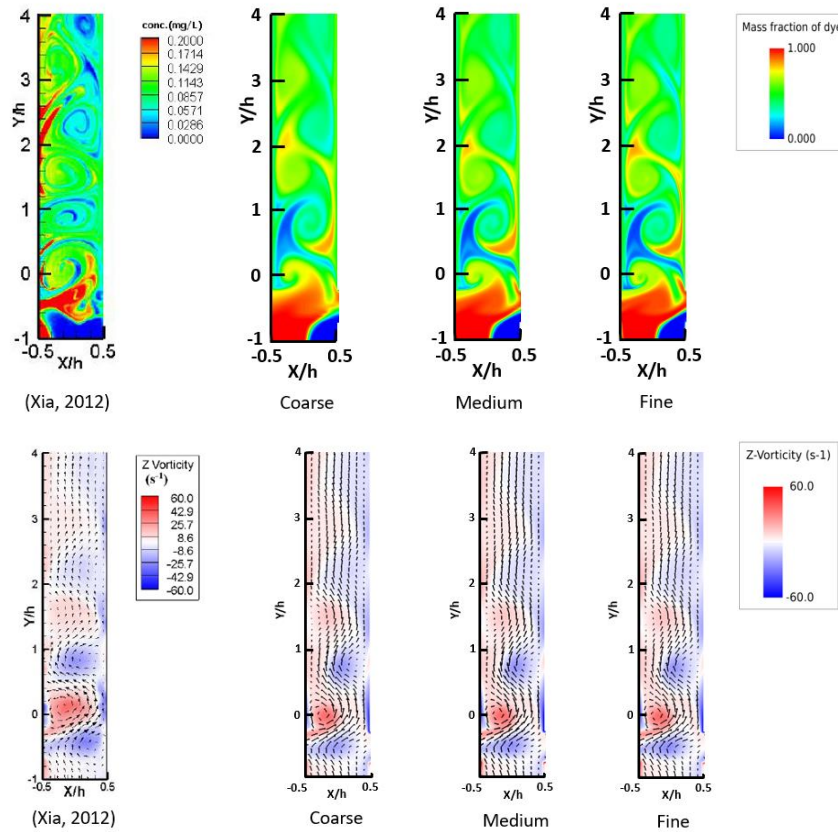
Fig. 5. Comparison of instantaneous concentration contours (upper), and phase-averaged velocity fields and vorticity contours (bottom) among experiment and three difference meshes. All the visualization results are captured around the orifice exit region at the end of ejection cycle of left SJA under stroke ratio, L = 4 and velocity ratio, R_v = 1.6
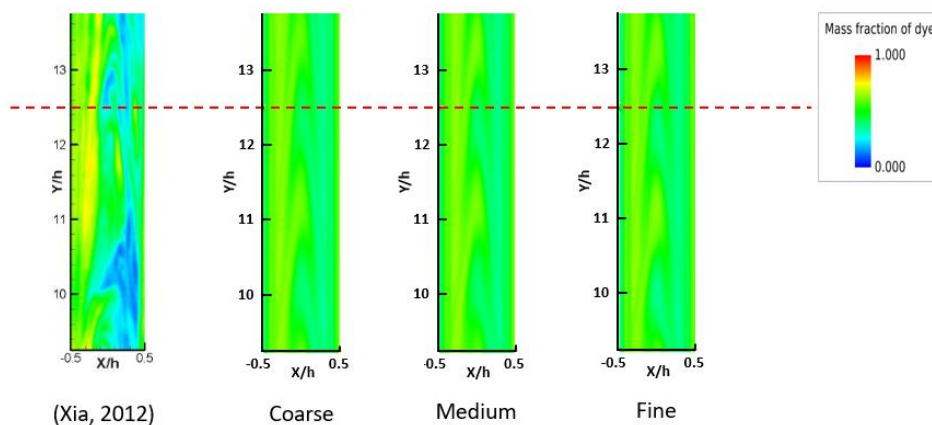
Fig. 6. Comparison of instantaneous concentration contours around the region of evaluation plane (red dot line) among experiment and three different meshes at stroke ratio, L = 4 and velocity ratio, R_v = 1.6

3.3 Time-step independence study

Three different time-step sizes are investigated in this study. Steps of 0.0025, 0.005 and 0.01 s are applied on the case with medium mesh sizes. Table 5 shows that the numerical results of 0.0025s has the smallest discrepancy as compared to the experimental data. As observed from Figure 7, at smaller time-step size, the time-averaged mixing degree predicted by CFD moves closer towards the experimental value. However, at the smallest time-step size, the discrepancy is still around 20% despite an increase in the computing time by 68.55% as compared to 0.005 s. It is expected that further reducing the delta t might improve the error. However, that would be infeasible given the limit of the available computation power.

Table 5
Time-averaged mixing degree obtained from cases with time-step sizes of 0.0025, 0.005 and 0.01s

Time-Step size (s)	Mixing degree [2]	Time-averaged mixing degree (Present study)	Percentage Difference (%)
0.0025	0.677	0.81	19.54
0.005	0.677	0.83	22.94
0.01	0.677	0.84	24.4
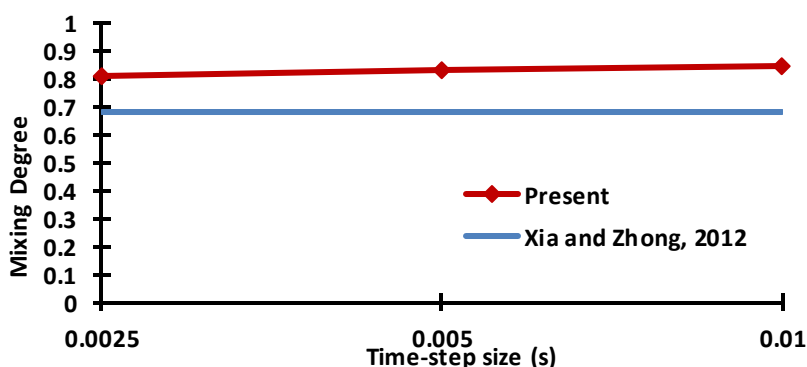
Fig. 7. Comparison of time-averaged mixing degree obtained from different time-step sizes (t = 0.0025, 0.005, 0.01 s) and experiment at stroke ratio, L = 4 and velocity ratio, R_v = 1.6

3.3.1 Near-field region

Figure 8 shows the instantaneous concentration contours and phase-averaged velocity vector fields obtained at the end of the ejection cycle of the left SJA under different time-step sizes. The contour visualization results show that the flow patterns of both fluids were captured in more detail as the time-step size decreases. Despite the difference in time-step sizes, the velocity vector fields depict that the vortex pair ejected from the LSJ orifices has similar size and propagation distance in all the cases as compared to the one in experiment from [16].
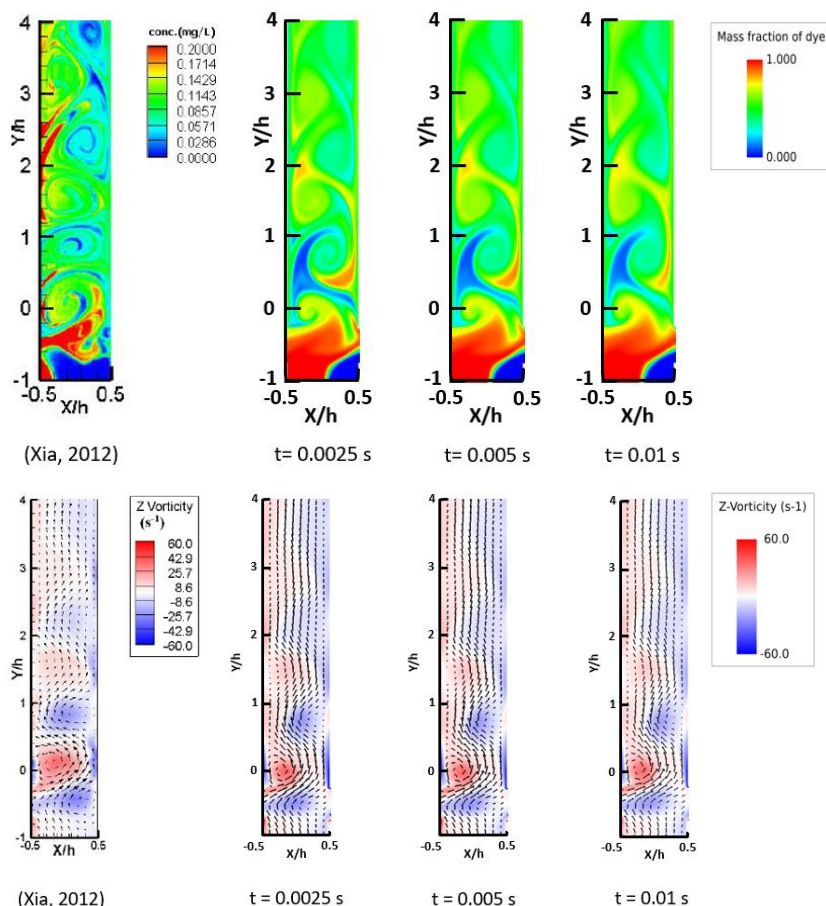
Fig. 8. A comparison of instantaneous concentration contours (upper), and phase-averaged velocity fields and vorticity contours (bottom) among experiment and different time-step sizes. All the visualization results are captured around the orifice exit region at the end of ejection cycle of left SJA under stroke ratio, L = 4 and velocity ratio, R_v = 1.6

3.3.2 Downstream flow region

Figure 9 depicts that the concentration contour near the region of evaluation plane do not affected by the applied time-step sizes. Besides, Figure 9 also confirms that the over predicted mixing degree (shown in Table 5) is attributed to the presence of larger well-mixed region (green) at the evaluation plane as compared to the one in experiment.

As the time step of 0.0025 s gives the best spatial resolution and computational accuracy, it is chosen for further investigation in the present study.

3.4 Validation of computational results

CFD simulation results obtained with the aforementioned numerical approaches, selected mesh partitions and time-step size are compared with the experimental data collected by Xia and Zhong [2]. As shown in Figure 10, both experimental data and CFD results show similar graph trend, which indicate that increasing the stroke ratio can significantly improve the time-averaged mixing degree. Despite the overprediction at L = 4, the time-averaged mixing degree predicted by CFD is lower than the experimental data under different stroke ratios. However, as the stroke ratio increases, the

discrepancy between CFD results and experimental data decreases, which leads to a good agreement at L = 8. These discrepancies will be further explained in Section 3.4.2.
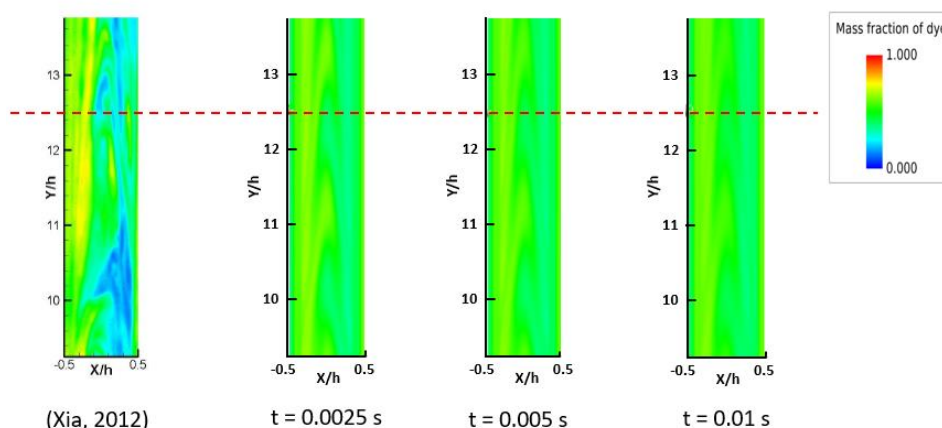
Fig. 9. A comparison of instantaneous concentration contours around the region of evaluation plane (red dot line) among experiment and different time-step sizes at stroke ratio, L = 4 and velocity ratio, R_v = 1.6
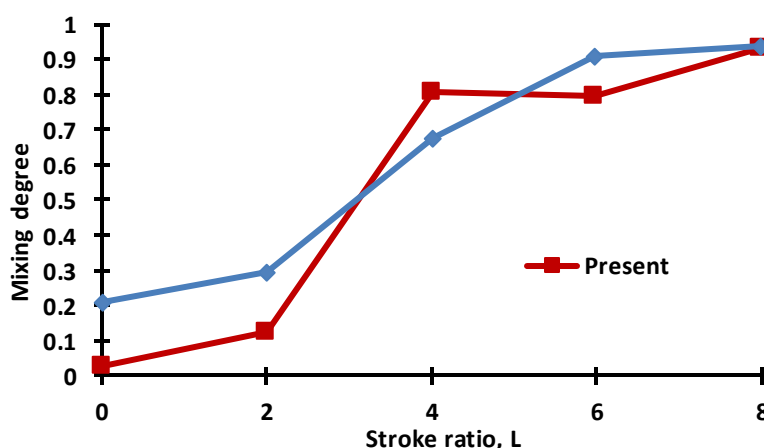
Fig. 10. Comparison of time-averaged mixing degree obtained from experiment and present study at different Stroke ratio, L

3.4.1 Near-field region

As shown in Figure 11, during the ejection cycle under L=2, the instantaneous concentration contour obtained from experiment shows small vortex structure from left SJA, which cannot be observed from the present study. In addition, the vortex structure ejected from the left SJA has been elongated in the present study as compared to the one in experiment. The phase-averaged velocity vector and vorticity contour in the same figure confirm the presence of the vortices in the flow field in both experiment and present study. Both studies have also show similar size of vortex pair ejected from left SJA.
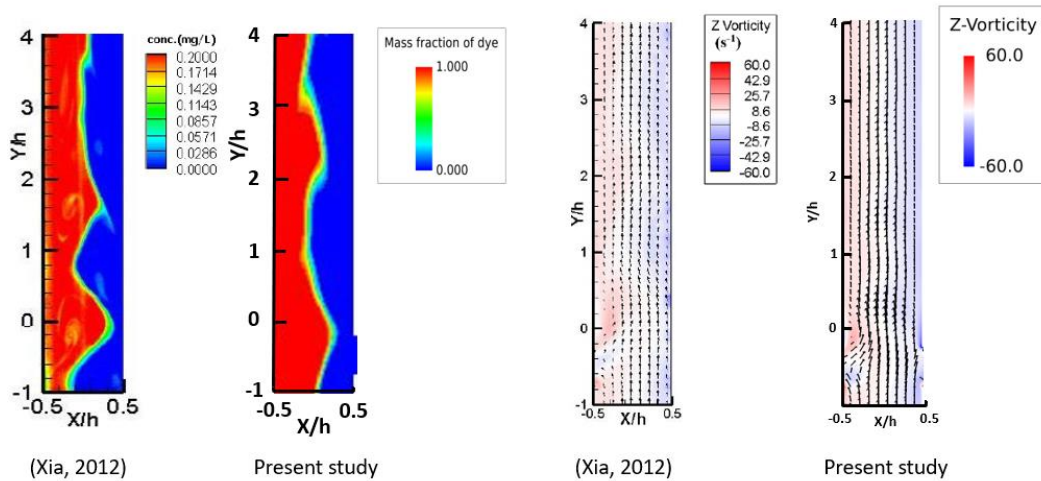
Fig. 11. Comparison between instantaneous concentration contours (left), and phase-averaged velocity vector and vorticity contours (right) obtained from experiment and present study. All the visualization results are captured near the orifice exit region at the end of ejection cycle of left SJA under stroke ratio, L = 2 and velocity ratio, R_v = 0.8

As observed in Figure 12, during the ejection cycle under L=6, the instantaneous concentration contour in the experiment shows a larger well-mixed region (green) along the mixing channel than the one in the present study. Besides, the flow pattern of the vortices depicted by the present study is not as apparent as the one in experiment. Moreover, the phase-averaged velocity vector and vorticity contour obtained from the present study shows that the vortex pair from the right SJA formed in the previous cycle is not destroyed by the vortex pair from the left SJA. Therefore, the vortex pair ejected from the left SJA is smaller in size as compared to the one in experiment.
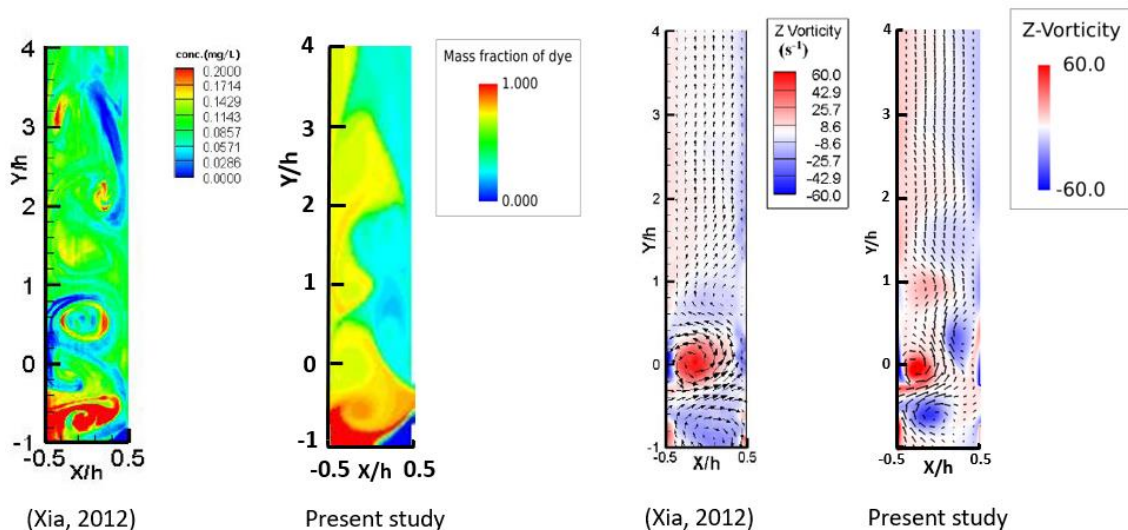
Fig. 12. Comparison between instantaneous concentration contours (left), and phase-averaged velocity vector and vorticity contours (right) obtained from experiment and present study. All the visualization results are captured near the orifice exit region at the end of ejection cycle of left SJA under stroke ratio, L = 6 and velocity ratio, R_v = 2.4

Under the condition of L = 8, the instantaneous concentration contours in Figure 13 shows that the vortex structure is not visible in both experiment and present study. Nonetheless, the phase-averaged velocity vector and vorticity contours depict the formation of strong vortex pair from the

left SJA in both studies. Despite smaller size of vortex pair ejected from the left SJA, the phase-averaged velocity vector and vorticity contours in the present study also show that the vortex pair ejected from the right SJA in the previous cycle has propagated further downstream than the one in experiment.
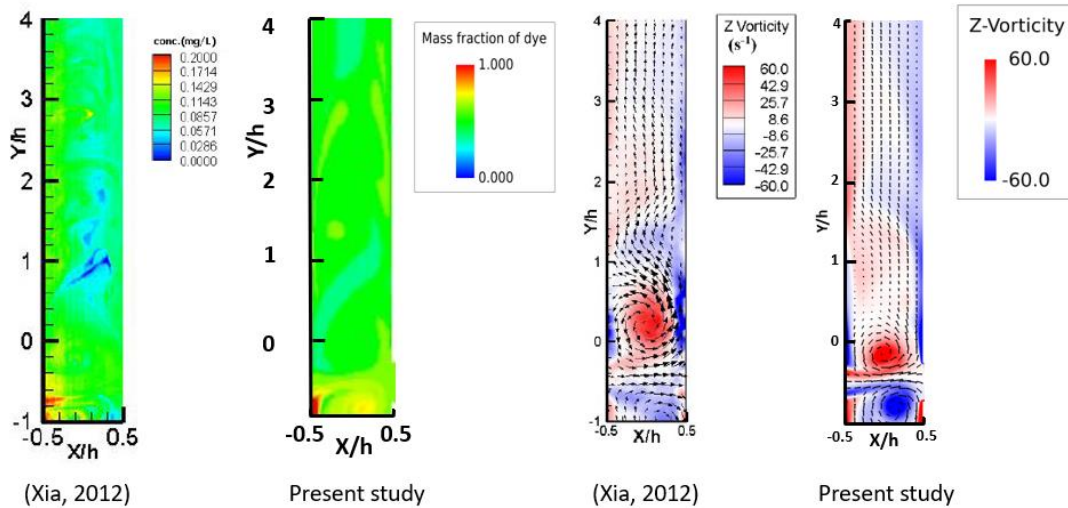
Fig. 13. Comparison between instantaneous concentration contours (left), and phase-averaged velocity vector and vorticity contours (right) obtained from experiment and present study. All the visualization results are captured near the orifice exit region at the end of ejection cycle of left SJA under stroke ratio, L = 8 and velocity ratio, R_v = 3.2

3.4.2 Downstream flow region

In order to explain the discrepancies of time-averaged mixing degree between the experimental data and present study (as shown in Figure 10), the downstream flow region around the evaluation plane is illustrated in Figure 14. As shown in Figure 14, the periodic 'A' shaped structure is evident in both experiment and present study for the case L = 2. In the experiment, the left flow stream (dye) is partially mixed (indicated by small yellow strips), which is not observed in the present study. Thus, an underpredicted time-averaged mixing degree is obtained by the present study in case L = 2 (as shown in Figure 10). Case L = 4 is not discussed here as it has been explained in Section 3.2.2 and 3.3.2. For case L = 6, the partially mixed strips are still evident in the present study, however, they are not observed in the experiment. This indicates that the right and left fluid streams are more concentrated around the downstream region as compared to the one in experiment. Similar to case L = 2, this phenomenon has led to a underpredicted time-averaged mixing degree than the experimental data. For case L = 8, the instantaneous concentration contour obtained by the experiment and present study are nearly identical as most of the region in the observation is homogenously green. Therefore, the time-averaged mixing degree is well validated against the experimental data under the case of L = 8.
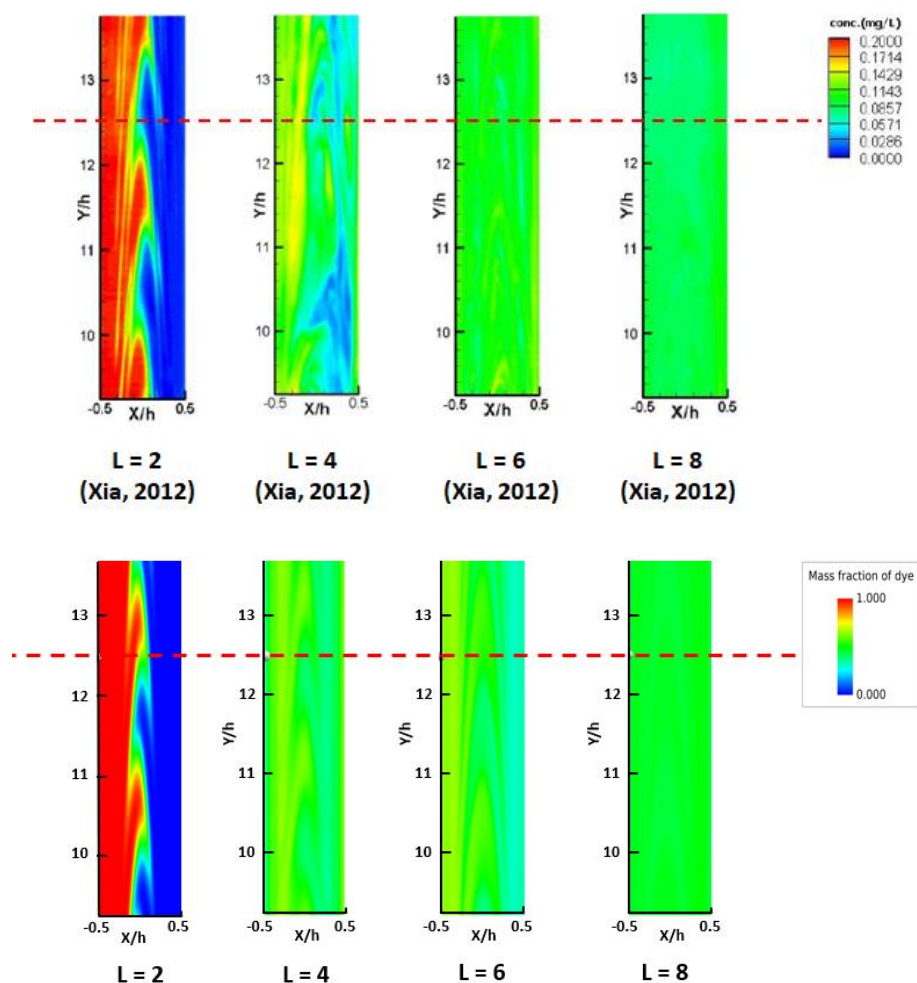
Fig. 14. Instantaneous concentration contours around the evaluation plane region (indicated by red dot line) shown by experiment [16] (upper), and present study (bottom) at different stroke ratios, L = 2, 4, 6 and 8, which corresponded to R_v = 0.8, 1.6, 2.4 and 3.2

4. Conclusions

A CFD model of synthetic-jet-assisted fluid mixer has been developed in the present study. The viscous laminar model and pressure-based solver is utilised to obtain the solution of unsteady incompressible flow 3D model. PISO scheme is chosen as the solution method while second order upwind scheme is chosen for the spatial discretization of pressure, momentum, dye and energy. First order implicit is used for the transient formulation. The simulation results show that this model is able to predict the time-averaged mixing degree reasonably well for a range of L, at max discrepancy around 20%. Moreover, the predictions at higher L values produce lower discrepancy. Based on the result of grid independence study, increasing the mesh density improves the spatial resolution of the visualization results, while gives negligible effect on the time-averaged mixing degree. For time-step independence study, increasing the time-step size worsen the spatial resolution of the visualization results and increases the percentage error between the experimental data and numerical results. Overall, the findings from this study produce some encouraging evidence for the capacity of numerical approach to simulate the jet characteristics in the aspect of mixing enhancement. Therefore, this approach can be used to replace the conventional experimental procedures for the ease of fabrication complexity and uncertainty of measurement.

Acknowledgement

References

[1]   Chen, Y., S. Liang, K. Aung, A. Glezer, and J. Jagoda. "Enhanced mixing in a simulated combustor using synthetic jet actuators." In *37th Aerospace Sciences Meeting and Exhibit,* p. 449. 1999.

[2]   Xia, Qingfeng, and Shan Zhong. "A PLIF and PIV study of liquid mixing enhanced by a lateral synthetic jet pair." *International Journal of Heat and Fluid Flow* 37 (2012): 64-73.

[3]   Xia, Qingfeng, and Shan Zhong. "Enhancement of laminar flow mixing using a pair of staggered lateral synthetic jets." *Sensors and Actuators A: Physical* 207 (2014): 75-83.

[4]   Xia, Qingfeng, and Shan Zhong. "Enhancement of inline mixing with lateral synthetic jet pairs at low Reynolds numbers: The effect of fluid viscosity." *Flow Measurement and Instrumentation* 53 (2017): 308-316.

[5]   Amitay, Michael, Douglas R. Smith, Valdis Kibens, David E. Parekh, and Ari Glezer. "Aerodynamic flow control over an unconventional airfoil using synthetic jet actuators." *AIAA journal* 39, no. 3 (2001): 361-370.

[6]   Amitay, Michael, and Florine Cannelle. "Evolution of finite span synthetic jets." *Physics of Fluids* 18, no. 5 (2006): 054101.

[7]   Mahalingam, Raghav, and Ari Glezer. "Design and thermal characteristics of a synthetic jet ejector heat sink." *Journal of Electronic Packaging* 127, no. 2 (2005): 172-177.

[8]   Pavlova, Anna, and Michael Amitay. "Electronic cooling using synthetic jet impingement." *Journal of heat transfer* 128, no. 9 (2006): 897-907.

[9]   Smith, Barton L., and Ari Glezer. "Jet vectoring using synthetic jets." *Journal of Fluid Mechanics* 458 (2002): 1-34.

[10]   Smith, Barton L., and Ari Glezer. "Vectoring of adjacent synthetic jets." *AIAA journal* 43, no. 10 (2005): 2117-2124.

[11]   Vukasinovic, Bojan, Daniel Brzozowski, and Ari Glezer. "Fluidic control of separation over a hemispherical turret." *AIAA journal* 47, no. 9 (2009): 2212-2222.

[12]   Vukasinovic, Bojan, Ari Glezer, Stanlislav Gordeyev, Eric Jumper, and Valdis Kibens. "Fluidic control of a turret wake: aerodynamic and aero-optical effects." *AIAA journal* 48, no. 8 (2010): 1686-1699.

[13]   L. N. Cattafesta, Q. Song, D. R. Williams, C. W. Rowley, and F. S. Alvi, "Active control of flow-induced cavity oscillations," *Prog. Aerosp. Sci.*, vol. 44, no. 7–8, pp. 479–502, 2008.

[14]   Tesař, V. "Oscillator micromixer." *Chemical Engineering Journal* 155, no. 3 (2009): 789-799.

[15]   Mautner, Thomas. "Application of the synthetic jet concept to low Reynolds number biosensor microfluidic flows for enhanced mixing: a numerical study using the lattice Boltzmann method." *Biosensors and Bioelectronics* 19, no. 11 (2004): 1409-1419.

[16]   Xia, Qingfeng. "Enhancement of liquids mixing using active pulsation in the laminar flow regime." PhD diss., The University of Manchester (United Kingdom), 2012.

[17]   Xia, Qingfeng, and Shan Zhong. "Liquids mixing enhanced by multiple synthetic jet pairs at low Reynolds numbers." *Chemical Engineering Science* 102 (2013): 10-23.

[18]   Wang, H., and S. Menon. "Fuel-air mixing enhancement by synthetic microjets." *AIAA journal* 39, no. 12 (2001): 2308-2319.

[19]   Beng, Soo Weng, and Wan Mohd Arif Aziz Japar. "Numerical analysis of heat and fluid flow in microchannel heat sink with triangular cavities." *Journal of Advanced research in fluid mechanics and thermal sciences* 34 (2017): 1-8.

[20]   Chan, Sze Qi, Fazlina Aman, and Syahira Mansur. "Bionanofluid Flow Through a Moving Surface Adapting Convective Boundary Condition : Sensitivity Analysis," *J. Adv. Res. Fluid Mech. Therm. Sci.*, vol. 54, no. 1, pp. 57–69, 2019.

[21]   Kumar, Jatinder, and Ajay Bansal. "CFD modeling of hydrodynamics and mass transfer of Rhodamine B in annular reactor." *Heat and Mass Transfer* 48, no. 12 (2012): 2069-2077.

[22]   Rani, Suriani Abdul, Betsey Pitts, and Philip S. Stewart. "Rapid diffusion of fluorescent tracers into Staphylococcus epidermidis biofilms visualized by time lapse microscopy." *Antimicrobial agents and chemotherapy* 49, no. 2 (2005): 728-732.

[23]   Glezer, Ari. "The formation of vortex rings." *The Physics of fluids* 31, no. 12 (1988): 3532-3542.

[24]   Smith, Barton L., and Ari Glezer. "The formation and evolution of synthetic jets." *Physics of fluids* 10, no. 9 (1998): 2281-2297.

[25]   Glasgow, Ian, and Nadine Aubry. "Enhancement of microfluidic mixing using time pulsing." *Lab on a Chip* 3, no. 2 (2003): 114-120.